

Discovery of a Potent and Selective Chikungunya Virus Envelope Protein Inhibitor through Computer-Aided Drug Design

Leandro Battini, Daniela M. Fidalgo, Diego E. Álvarez,^{*,§} and Mariela Bollini^{*,§}Cite This: *ACS Infect. Dis.* 2021, 7, 1503–1518

Read Online

ACCESS |



Metrics & More



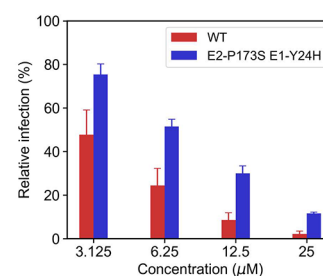
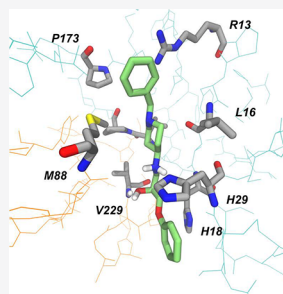
Article Recommendations



Supporting Information

ABSTRACT: The worldwide expansion of chikungunya virus (CHIKV) into tropical and subtropical areas in the last 15 years has posed a currently unmet need for vaccines and therapeutics. The E2-E1 envelope glycoprotein complex binds receptors on the host cell and promotes membrane fusion during CHIKV entry, thus constituting an attractive target for the development of antiviral drugs. In order to identify CHIKV antivirals acting through inhibition of the envelope glycoprotein complex function, our first approach was to search for amenable druggable sites within the E2-E1 heterodimer. We identified a pocket located in the interface between E2 and E1 around the fusion loop. Then, via a structure-based virtual screening approach and in vitro assay of antiviral activity, we identified compound 7 as a specific inhibitor of CHIKV. Through a lead optimization process, we obtained compound 11 that demonstrated increased antiviral activity and low cytotoxicity (EC_{50} 1.6 μ M, CC_{50} 56.0 μ M). Molecular dynamics simulations were carried out and described a possible interaction pattern of compound 11 and the E1-E2 dimer that could be useful for further optimization. As expected from target site selection, compound 11 inhibited virus internalization during CHIKV entry. In addition, virus populations resistant to compound 11 included mutation E2-P173S, which mapped to the proposed binding pocket, and second site mutation E1-Y24H. Construction of recombinant viruses showed that these mutations conferred antiviral resistance in the parental background. Finally, compound 11 presents acceptable solubility values and is chemically and enzymatically stable in different media. Altogether, these findings uncover a suitable pocket for the design of CHIKV entry inhibitors with promising antiviral activity and pharmacological profiles.

KEYWORDS: *chikungunya, virtual screening, envelope glycoproteins, entry inhibitors, aminopiperidines and -piperidine analogues*



Chikungunya virus is an alphavirus in the family *Togaviridae* that is transmitted to humans by *Aedes* spp. mosquitoes. Infection often causes acute fever and joint pain. In some patients, joint pain persists in subacute and chronic forms of the disease. The virus has rapidly moved in recent years from Africa to Islands of the Indian Ocean and finally to India, causing 1.9 million cases since 2007. In 2007, a localized outbreak was reported in Europe, and since 2013 local transmission has occurred in the Americas with around 3 million suspected cases and nearly 150 (2017–2020) deaths attributed to the disease.¹ Due to the lack of effective countermeasures, CHIKV has been prioritized under the World Health Organization blueprint for research and development including the study of basic aspects of virus biology and the design of antiviral strategies.

Chikungunya virus particles are composed of heterodimers of E1 and E2 transmembrane proteins, a host derived lipid bilayer, and the nucleocapsid associated with a single copy of the RNA genome. E2 and E1 are the products of maturation and processing of the structural polyprotein of chikungunya that encompasses capsid protein (cp), the p62 precursor of envelope proteins E3 and E2, 6K, and envelope protein E1. Two hundred and forty copies of the heterodimer that form E2

and E1 are exposed on the surface of the virus as trimeric spikes.²

The entry of chikungunya virus is mediated by envelope glycoproteins E2 and E1 that are responsible for receptor binding and fusion, respectively. Chikungunya virus uses clathrin-mediated endocytosis as the entry pathway, and fusion is triggered by the acidic pH of the endocytic vesicle.^{2,3} The result of this process is the release of the RNA genome into the cell cytoplasm, allowing the translation of viral proteins and the replication of the genome.

The crystal structure of the chikungunya envelope heterodimer, together with structural and functional studies of envelope proteins of other alphaviruses, has uncovered the mechanism of virus fusion.⁴ E1 displays a three domain (I, II, and III) architecture folding with a β -barrel structure, and E2

Special Issue: Antiviral Therapeutics

Received: January 4, 2021

Published: May 28, 2021



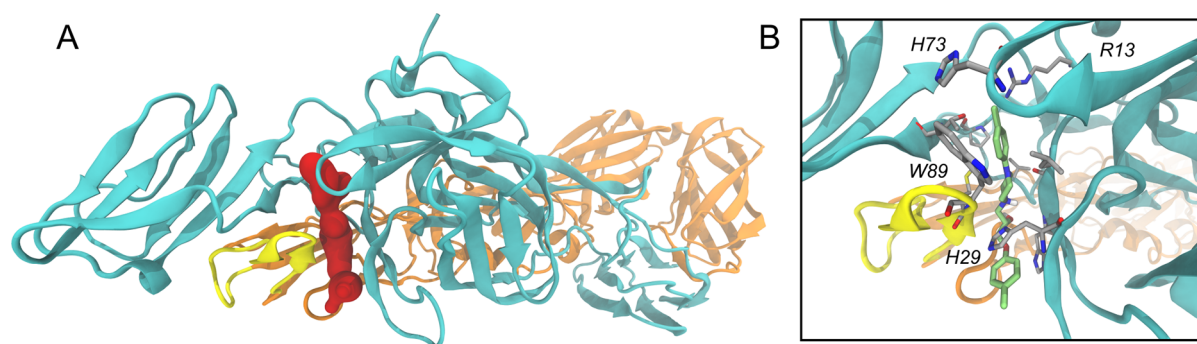


Figure 1. Binding site identification and virtual screening hit. (A) Representation of the crystal structure of the envelope proteins of CHIKV E1 (orange) and E2 (cyan) (PDB 3N42). The fusion loop is represented as yellow ribbons, and the selected binding site (pocket A) is represented as a red surface. (B) Docking model of compound 7 in complex with the E1-E2 dimer. The compound is represented as green sticks, and relevant side chains for the protein ligand interaction are colored in gray.

belongs to the immunoglobulin superfamily with three domains (A, B, and C). In the E2-E1 complex, contacts between envelope proteins occur by lateral interactions involving domain II of E1. At neutral pH, a groove between domains A and B of E2 accommodates the fusion peptide, preventing premature activation of fusion. Fusogenic activity of E1 requires a low pH that triggers a conformational change in E2. Domain B moves out of domain A, exposing the fusion peptide located in E1.⁵

Envelope proteins are attractive targets for the design of antiviral therapies, and inhibition of envelope proteins function represents a specific strategy to block virus entry into the host cell. In fact, envelope proteins are the targets of small molecules currently in phase II clinical trials that block HIV entry⁶ and of peptide and antibody entry inhibitors that are approved in the treatment of HIV, respiratory syncytial virus, and varicella zoster virus infections. In the case of chikungunya, approved drugs such as chloroquine and Arbidol display modest antiviral activity as entry inhibitors acting by raising the endosomal pH and interfering with receptor binding, respectively.^{7,8} In turn, the antiparasitic drug suramin inhibits fusion of chikungunya acting on the virus envelope proteins.⁹ Combined selection and characterization of suramin resistant virus variants, and docking to the trimeric spike indicate that suramin interacts with a flexible loop in the N-terminus of one E2 molecule, while it extends toward the middle of domain A of an adjacent E2.^{9,10} Finally, identification of envelope protein inhibitors through virtual screening approaches has been reported, but hits were not characterized for antiviral activity *in vitro*.^{11,12}

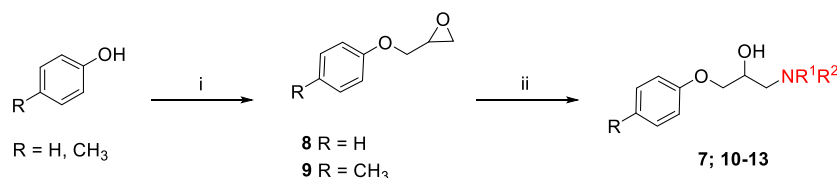
Here, we used computer guided drug design and *in vitro* screening of antiviral activity to identify small-molecule ligands of the CHIKV E2-E1 heterodimer in a pocket lying in the interface between E2 and E1 around the fusion loop. The approach led to the design of an aminopiperidine analogue (compound 11) that showed specific anti CHIKV activity in the low micromolar range and acted through the inhibition of internalization during virus entry. The emergence of mutations on the envelope proteins associated with resistance to the antiviral activity of the compound supported the proposed molecular target. Additionally, a possible interaction pattern of compound 11 and E1-E2 heterodimer was described with molecular dynamics (MD) simulations and compound 11 showed adequate solubility and stability on *in vitro* assays. Overall, these data provide novel experimental insight into the

rational design of CHIKV entry inhibitors and encourage further optimization of the identified antiviral compound.

RESULTS

Identification of CHIKV Inhibitors through Virtual Screening. In order to identify CHIKV entry inhibitors, we carried out a structure-based virtual screening using the crystal structure of mature CHIKV envelope proteins as a receptor (PDB 3N42).⁴ To detect potential drug binding pockets in the protein surface, we used three different software applications that search binding sites according to different criteria. We identified a binding site that was well ranked by all programs and that also had biological relevance (pocket A, Figure 1A). Pocket A is located behind the fusion loop of E1 in a cleft formed between domain II of E1 and domains A and B of E2. This region is important for the fusion between the viral envelope and the endosome membrane during internalization of the viral particle.⁴ Pocket A has 52% hydrophobic residues and a volume of 592 Å³ according to FPocket. Furthermore, Pocket A is stable in a molecular dynamics simulation of CHIKV envelope proteins (Figure S19D and E). Key residues that may establish interactions with druglike molecules include hydrogen bond donors and acceptors (E2-S27, E2-T175, E2-N231, E2-Q236, and E1-T228) and aromatic residues involved in π - π interactions (E2-H18, E2-H29, E2-H73, and E1-W89). Due to the adequate physicochemical properties and biological relevance, we choose pocket A to carry out the virtual screening.

We performed the virtual screening of Chembridge (~650 000 compounds)¹³ and NCI (~265 000 compounds)¹⁴ databases against pocket A. Before docking, we filtered the molecules by their chemical similarity and predicted toxicity and absorption, distribution, metabolism, and excretion (ADMET) properties. Then, we obtained a database with ~880 000 compounds which were subjected to high throughput docking with three types of docking software. First, we docked molecules with AutoDock Vina¹⁵ and compounds that did not enter into the binding pocket were discarded. Filtered molecules (~176 000 molecules) were additionally docked with LeDock¹⁶ and AutoDock4¹⁷ and were ranked by exponential consensus ranking¹⁸ (Figure S17). The predicted structures of the complexes for the top scoring 1% drugs received extensive scrutiny. First, scaffold diversity was taken into consideration using ChemMine tools.¹⁹ Then, each group of similar compounds were inspected based on intermolecular contacts with the key amino acids described

Scheme 1. Synthesis of Compounds 7 and 10–13^a

^aReagents and conditions. (i) epichlorohydrin, 1 M aqueous NaOH, THF, rt, 5 days; (ii) NHR¹R², MeOH, rt, 48 h.

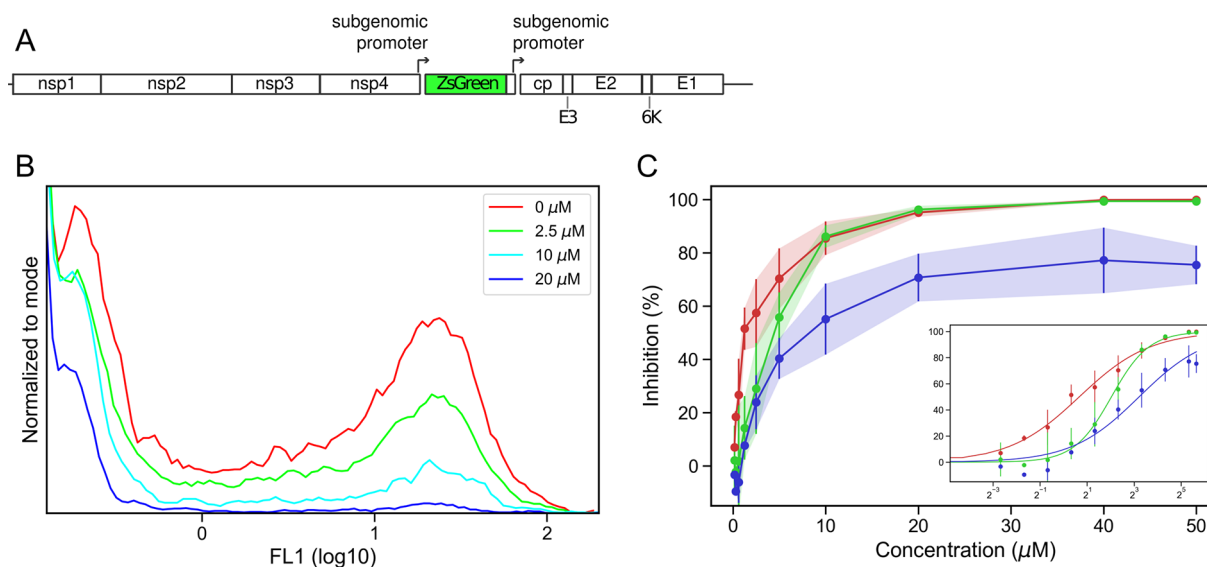


Figure 2. Antiviral activity optimization of compound 7. (A) Schematic representation of CHIKV-ZsGreen genome. ZsGreen is expressed in the cell cytoplasm as the product of translation of a subgenomic RNA inserted between the ORFs encoding for virus non structural and structural proteins. (B) Representative histograms of ZsGreen fluorescence obtained with flow cytometry of Vero cells infected with CHIKV-ZsGreen and treated with compound 11. (C) Antiviral activity of compound 7 derivatives (blue for compound 7, green for compound 10, and red for compound 11). Vero cells were infected with CHIKV-ZsGreen with a MOI of 0.01 and treated with serial dilutions of each derivative. One day post infection, the percentage of infected cells was determined by flow cytometry and the inhibition for each compound concentration was calculated in comparison to the untreated control. Values represent the mean and standard error of three independent experiments. The EC₅₀ for each compound was calculated from a nonlinear curve fit of the data, shown in the inset.

above, adequate druglike predicted properties, consensus ranking, and synthetic feasibility for further modifications (Figures S16 and S17). Finally, compounds 1–6 were bought and compound 7 was synthesized following the synthetic route described in Scheme 1.

Next, we measured antiviral activity and cytotoxicity of the selected compounds in cell-based assays. To measure antiviral activity, we used a reporter CHIKV variant of the Indian Ocean lineage that encodes for ZsGreen as the product of translation of a subgenomic RNA (CHIKV-ZsGreen, Figure 2A).²⁰ Cells infected with this virus express ZsGreen in the cytoplasm, so virus replication can be scored by detection of fluorescence. To screen for antiviral activity of the selected compounds, we infected Vero cells with CHIKV-ZsGreen with a multiplicity of infection (MOI) of 0.01 and treated the cells at two drug concentrations. At 24 h after infection we measured the percentage of infected cells by flow cytometry (Table 1). Among the tested compounds, only compound 7 showed antiviral activity and no visible cytotoxicity at the evaluated concentrations. The estimated effective concentration 50 (EC₅₀) of compound 7, *i.e.*, the concentration of compound that inhibits the viral infection by 50%, was $9.3 \pm 1.7 \mu\text{M}$ (Figure 2C), and no cytotoxicity was observed after the treatment with 100 μM or lower concentrations of the compound (Table 2). Altogether, our virtual screening

approach targeting the envelope proteins of the virus led to the identification of an inhibitor of CHIKV.

Lead Optimization of 7, Synthesis, and Antiviral Activity. To date, antiviral targeting of the E2-E1 heterodimer has only been demonstrated for a small number of molecules that inhibit virus entry and were confirmed by the selection of resistant variants in cell culture, which harbor mutations in E2 or E1.⁶ To gain insight into key structural features that can be associated with antiviral activity, we aimed at modifying compound 7. We synthesized four compounds (10–13) in which the terminal *N*-phenyl ring was replaced by *N*-benzyl (10) and *N*-methyl group (12). In addition, the central piperazine heterocyclic ring was replaced by an aminobiphenyl group in (13). Finally, the piperazine group was replaced by amino piperidine group (11). The synthesis of the desired β -amino alcohols 7 and 10–13 proceeded via two steps as shown in Scheme 1. First, phenol or 4-methyl phenol sodium salt reacted with epichlorohydrin to yield the corresponding phenyl glycidyl ether (8 and 9, respectively). Then, desired compounds were synthesized via the ring-opening of epoxides with a variety of amines (*N*-substituted piperazines, 4-aminopiperidine derivatives, and 4-biphenylamine). The final compounds were obtained with 20–53% yield after purification by recrystallization (EtOH, MeOH, or EtOH/

Table 1. Anti-CHIKV Activity of Selected Compounds^a

Structure	Compd. ID	% inhibition	
		10 μ M	50 μ M
	1	0	6.6
	2	20.9	ND*
	3	0	1.7
	4	0	4.7
	5	0	0
	6	0	0
	7	55.1	75.1

^aCells were infected with CHIKV-ZsGreen and treated with virtual screening hits at the indicated concentrations. Inhibition of CHIKV replication was calculated as the ratio of the percentages of ZsGreen positive cells between treated cells and the untreated cells control.

Table 2. Cytotoxicity and Anti-CHIKV Activity of Selected Compounds^a

Structure	ID	EC ₅₀ (μ M)	CC ₅₀ (μ M)	SI
	7	9.3 \pm 1.7	>100	>10.8
	10	4.1 \pm 0.6	36.2 \pm 2.6	8.8
	11	1.6 \pm 0.3	56.0 \pm 4.7	35
	12	NA	>100	NA
	13	NA	>100	NA

^aEC₅₀: compound concentration that reduces the percentage of infected cells by 50%. CC₅₀: compound concentration that reduces cell viability by 50% as assessed by MTT assay. Data are expressed as mean values \pm SE from at least 3 independent experiments. SI: CC₅₀/EC₅₀: *In vitro* selectivity index; NA: No active compound.

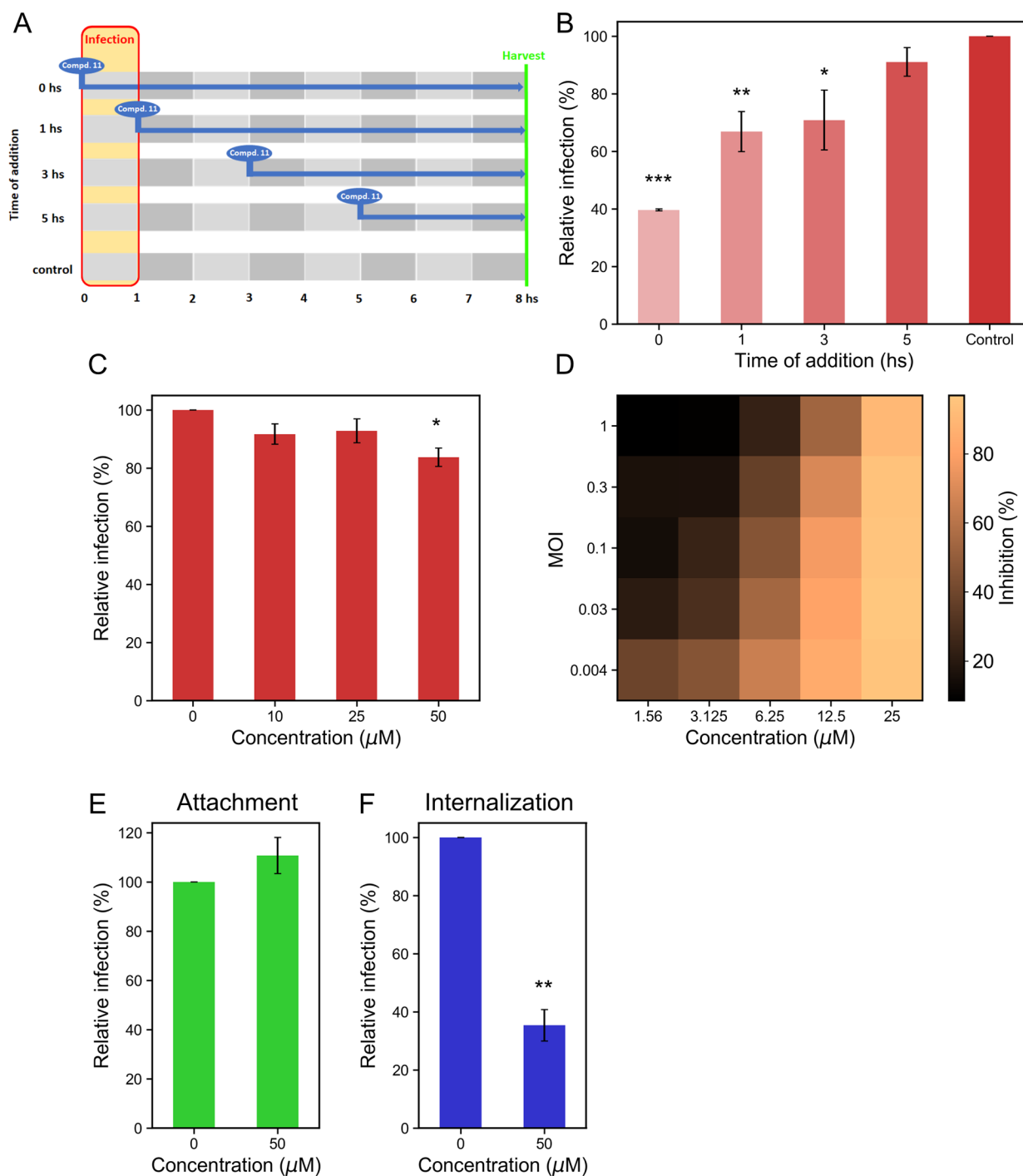


Figure 3. Study of the mechanism of action of compound 11. (A) Schematic representation of the time of drug addition experiment. Compound 11 was added at the time points indicated in the scheme, during or after infection with CHIKV-ZsGreen. Virus yields were assessed in cell culture supernatants harvested after a single cycle of replication and used to infect a new cell monolayer. The percentage of infected cells was determined by flow cytometry and relativized to the nontreated control as a measure of virus yields. (B) Bar graph showing the percentage of infected cells after infection with virus supernatants harvested following the time of drug addition scheme. Bars represent the mean and standard error of three independent experiments. Asterisks indicate a statistically significant difference in comparison with the nontreated control (one-way ANOVA with Dunnett's post test. $*P \leq 0.05$, $**P \leq 0.01$, $***P \leq 0.001$). (C) Compound 11 has no virucidal effect. CHIKV-ZsGreen was incubated with compound 11 for 1 h at 37 °C and then used to infect Vero cells at a MOI of 0.01, after diluting 11 to a nonactive concentration (100-fold). One day post infection, the percentage of infected cells was determined by flow cytometry and relativized to the nontreated control (one-way ANOVA with Dunnett post test. $*P \leq 0.05$). (D) Effect of compound 11 is MOI dependent. Vero cells were treated with different concentrations of 11 and infected with CHIKV-ZsGreen at different MOIs. One day post infection, the percentage of infected cells was determined by flow cytometry and the inhibition for each treatment was calculated in comparison to the untreated control for each MOI. The heat map represents the mean inhibition of three independent experiments. (E) Compound 11 has no effect on CHIKV attachment. Vero cells were infected with CHIKV-ZsGreen, and virus attachment was allowed to proceed in the presence of 11. Attached virus was recovered by cell lysis and used to infect a new monolayer of cells. The percentage of infected cells was determined by flow cytometry and relativized to the nontreated

Figure 3. continued

control. Bars represent the mean and standard error of three independent experiments (paired *t* test; control vs compound **11**, not significant). (F) Compound **11** inhibits the internalization of CHIKV. Vero cells were infected with CHIKV-ZsGreen and, following virus attachment, treated with **11** during internalization, harvested, and plated onto a new cell monolayer. The percentage of infected cells was determined by flow cytometry and relativized to the nontreated control. Bars represent the mean and standard error of three independent experiments. Asterisks indicate a statistically significant difference in comparison with the nontreated control (paired *t* test; control vs compound **11**, $**P \leq 0.01$).

H₂O mixtures) or silica gel chromatography (CH₂Cl₂/MeOH 9:1).

Antiviral assays showed that activity of compounds **10** and **11** was higher compared to the lead compound **7**, with EC₅₀ values of 4.6 and 1.6 μM, respectively (Figure 2C and Table 2). The substitution of phenyl ring by the 3-chloro benzyl group (**10**) had a major contribution to antiviral activity. However, substitution of the piperazine ring (**12**) with a small group such as methyl abolished the antiviral activity, suggesting that a bulky group contributes to the activity in this group of compounds. In turn, replacement of the heterocycle central ring by the aminobiphenyl group (**13**) also abolished antiviral activity, pointing to the importance of the heterocyclic ring in the central position of the molecule. Finally, the bioisosteric replacement of the piperazine group by amino piperidine (**11**) resulted in a slight increase in potency. Besides, this series of compounds showed considerably low cytotoxicity.

Compound 11 Inhibits the Early Stages of the CHIKV Replication Cycle Probably Acting on a Viral Target. We selected the most active compound, compound **11**, for the study of the mechanism of action of this series of molecules. According to the proposed target, the envelope proteins of CHIKV, we expected the compound to be active in the early stages of the viral life cycle. In order to test this hypothesis, we carried out a time of drug addition experiment. In this experiment, Vero cells were infected with CHIKV-ZsGreen at a MOI of 0.1 and the infection was allowed to proceed for 1 h before thoroughly washing the monolayer to synchronize infection. For treatment at 0 h, compound **11** was added simultaneously with the virus and replaced after washing the cells. For the rest of the treatments, compound **11** was added at a final concentration of 30 μM at different time points along the infection cycle. At 8 h post infection, the virus in the supernatant was harvested, diluted to a nonactive concentration of **11**, and used to infect a new monolayer of cells (Figure 3A). After 2 days, the percentage of infected cells was measured by flow cytometry (Figure 3B). The alphavirus life cycle is approximately 6–8 h long,²¹ so in this experiment we evaluated the effect of **11** in a single cycle of viral replication. When compound **11** was added with the virus inoculum during the infection, we observed a 60% reduction in the percentage of infected cells compared to the untreated control. This effect decreased when the compound was added at later time points after infection, suggesting that the compound has to be present in the early stages of the replication cycle in order to inhibit CHIKV replication.

To assess the direct effect of compound **11** on a viral target, we first performed a virucidal activity assay. To this end, we incubated CHIKV-ZsGreen with different concentrations of **11** for 1 h at 37 °C and then infected Vero cells after diluting **11** to a nonactive concentration. One day post infection, we measured the percentage of infected cells and we observed only a slight decrease of the infection after treatment with 50 μM **11** (16%), which may be explained by the remaining amount of compound (0.5 μM), therefore ruling out the

virucidal effect (Figure 3C). As a complementary approach, we tested whether the antiviral activity of **11** was MOI dependent. As expected for an antiviral acting directly on a viral target, we observed that the inhibition of infection by compound **11** decreased as MOI increased (Figure 3D).

Taken together, these results are in agreement with the proposed target for this series of compounds and suggest that compound **11** acts on a viral target during the early stages of CHIKV replication cycle, presumably during virus entry.

Compound 11 Inhibits the Internalization Step of the Viral Entry into the Host Cells. We next set out to discriminate the effect of compound **11** on attachment and internalization steps of CHIKV entry. To determine the effect of **11** in the attachment of the viral particle, Vero cells were infected with CHIKV-ZsGreen at a MOI of 0.1 and treated with 50 μM **11**. Virus was allowed to bind to the cell surface for 30 min at room temperature. After the attachment of the virus, cells were washed to remove the nonattached virus, and the attached virus was harvested by cell lysis. Fresh Vero cells were infected with the clarified cell lysate, and 48 h later the percentage of infected cells was measured by flow cytometry. In this experiment, the treatment with **11** had no effect in comparison with the untreated control (Figure 3E), indicating that the compound is not inhibiting the attachment of the virus to the cells.

Next, to determine the effect of compound **11** in the internalization step, Vero cells were infected with CHIKV-ZsGreen at a MOI of 0.1 in the absence of drug and the virus was allowed to bind to the cell surface for 30 min at room temperature. After attachment, cells were washed to remove the nonattached virus and were treated with 50 μM **11**. Following 1 h at 37 °C to allow the internalization of the attached virus, cells were treated with trypsin, collected, and plated onto a fresh monolayer of Vero cells. After 48 h, the percentage of infected cells was measured by flow cytometry (Figure 3F). Compared with the untreated control, the percentage of infected cells treated with **11** during the internalization step was reduced by 60%. This result shows that compound **11** is inhibiting the internalization step of CHIKV entry into the host cells.

Mutations in the Envelope Protein Are Selected after Serial Passage of CHIKV in the Presence of Compound 11. In order to gain experimental evidence that envelope proteins are the target of compound **11**, we carried out the selection of a viral population resistant to the antiviral activity of the compound. We expected that mutations on the envelope protein near the proposed binding pocket would arise in this population. To this end, we did 14 serial viral passages of CHIKV-LR in Vero cells infecting with a MOI of 0.01 and gradually increasing **11** concentration, from 5 to 50 μM. Fourteen serial viral passages in the absence of compound were done in parallel as a control to detect mutations that result from adaptation to cell culture passaging. At the end of the experiment, we measured the antiviral activity of **11** against

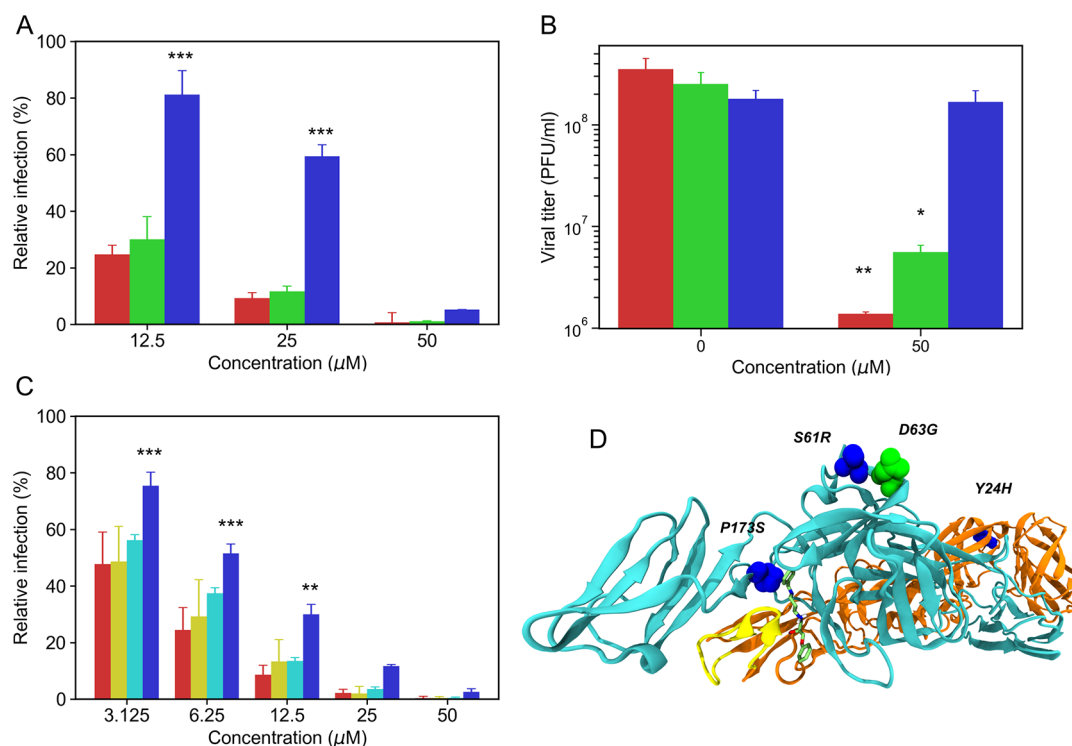


Figure 4. Selection of a resistant CHIKV population to the antiviral activity of compound **11**. (A, B) The sensitivity of WT CHIKV (red) or virus populations selected in the presence (blue) or absence (green) of **11** was assessed. (A) Vero cells were infected with each population and treated with different concentrations of **11**. After 24 h, cells were immunostained with an anti-E2 antibody and the percentage of infected cells was determined by flow cytometry and relativized to the nontreated control. The values represent the mean and standard error of three independent experiments. Asterisks indicate a statistically significant difference for each concentration in comparison with WT virus (two-way ANOVA with Bonferroni post test; $***P \leq 0.001$). (B) Vero cells were infected and treated with 50 μM **11**. Two days post infection, the viral yield was determined by plaque assay. Bars represent the mean and standard error of three independent experiments. Asterisks indicate a statistically significant difference for each virus in comparison with the nontreated control (two-way ANOVA with Bonferroni post test; $*P \leq 0.05$, $**P \leq 0.01$). (C) Sensitivity of WT CHIKV-ZsGreen (red), E1-Y24H (green), E2-P173S (cyan), or E1-Y24H E2-P173S (blue) mutant variants to compound **11**. Vero cells were infected with each variant and treated with different concentrations of **11**. One day post infection, the percentage of infected cells was determined by flow cytometry and relativized to the nontreated control. Values represent the mean and standard error of three independent experiments. Asterisks indicate a statistically significant difference for each concentration in comparison with WT virus (two-way ANOVA with Bonferroni post test; $***P \leq 0.001$, $**P \leq 0.01$). (D) Mapping of mutations detected in the population adapted in the presence (blue) or absence (green) of compound **11** in the crystal structure of the E1-E2 dimer.

each of the passaged populations and sequenced the envelope region of CHIKV genome by Sanger sequencing.

To test the antiviral activity of compound **11** against the selected viral populations, we infected Vero cells at a MOI of 0.01 with both adapted populations and with a wild type (WT) CHIKV stock recovered after transfection of in vitro transcribed genomic RNA and treated the cells with different concentrations of **11**. At 24 h after the infection, we harvested the cells and immunostained the infected cells with an anti-E2 antibody. We measured the percentage of infected cells by flow cytometry (Figure 4A). For all the evaluated concentrations, the percentage of infected cells is higher for the viral population selected in the presence of **11** compared to the WT virus, indicating that the selected population is resistant to the biological activity of this compound. Moreover, no significant differences were observed between the WT virus and the population adapted in the absence of **11**, suggesting that the emergence of resistance is due to the adaptation of the virus to compound **11** and not a consequence of the adaptation to passage in cell culture.

As a complementary approach, we determined the virus yield of each viral population in the absence of **11** or after the treatment with 50 μM of the compound. We determined the

virus yield in the supernatant 48 h after the infection by plaque assay (Figure 4B). In agreement with the previous results, there was no significant difference in the virus yield after the treatment with **11** in comparison to the untreated control for the population adapted in the presence of compound **11**. In contrast, with the cell culture adapted and the WT viruses, there was, respectively, a 50- and 100-fold reduction in the virus yield after treatment with the compound, further supporting that antiviral resistance does not arise from virus passaging in cell culture. In sum, we selected a population of CHIKV partially resistant to the action of compound **11** that emerged as the result of adaptation to the compound.

To identify mutations that emerged in the viral populations adapted in the absence or presence of compound **11**, we sequenced the envelope region of CHIKV genome by Sanger sequencing after the scheme of selection was completed. We detected a single amino acid substitution in the population adapted in the absence of **11**, D63G in E2. In the population adapted in the presence of compound **11**, we detected three mutations, E2-S61R, E2-P173S, and E1-Y24H (Figure 4D). On the one hand, E2-S61R is found in the same motif as the E2-D63G substitution selected in the population adapted in the absence of compound and it probably represents an

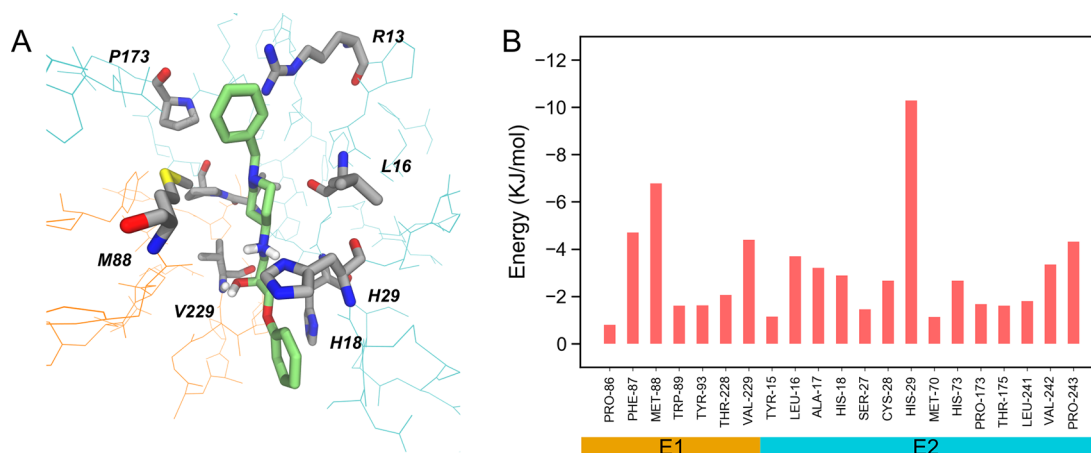


Figure 5. Molecular dynamics simulations of CHIKV envelope proteins in complex with compound **11**. (A) Representation of the central structure of the most populated cluster of the three molecular dynamics simulations of **11** in complex with the WT envelope proteins. Compound **11** is represented as green sticks and the most relevant amino acids are represented as gray sticks. Other nearby residues are represented as lines; orange for E1, and cyan for E2. (B) Contribution of neutral amino acids to the binding energy determined by the MMPBSA method. Bar represents the mean energy contribution of three replicates for the 21 residues with larger binding energy contribution.

adaptive substitution to virus growth in cell culture. On the other hand, E2-P173S is located in the proposed binding pocket (pocket A) and E1-Y24H is located in the hinge between domain I and domain III of E1. To assess if these mutations account for the resistance to compound **11** observed in the adapted viral population, we cloned E2-P173S and E1-Y24H separately or in combination in the CHIKV-ZsGreen WT background and determined the antiviral activity of compound **11** against the WT and the mutant variants (Figure 4C). No difference was observed for any of the single mutants with respect to the WT virus. In contrast, the E2-P173S E1-Y24H double mutant did show partial resistance to the compound. Indeed, the resistance phenotype of the recombinant double mutant virus reproduced that of the adapted viral population, showing a fold increase of infection with respect to the WT virus that was similar for the double mutant and the adapted viral population at different drug concentrations (approximately 3-fold at 12.5 μM and 6-fold at 25 μM). These results showed that mutations on the envelope proteins confer partial resistance to CHIKV to the antiviral activity of compound **11**, suggesting that the E1-E2 dimer may be the target of the compound. However, further work is needed to pinpoint compound **11** target to pocket A.

Description of the Interaction between Compound 11 and the Envelope Proteins of CHIKV through Molecular Dynamics Simulation. In order to describe the possible interactions between compound **11** and the E1-E2 proteins we performed molecular dynamic simulations. As a starting structure, we used the ligand protein complex obtained after docking. We used a reduced model of the E1-E2 dimer, which included the tip of domain II of E1 and the domains A, B and the β -ribbon of E2 embedded in the viral spike (Figure S18). We performed three simulations of 250 ns of E1-E2 in complex with compound **11** and one simulation of the apo protein. In all simulations, the protein remained stable (Figure S19A) and **11** remained within pocket A in a conformation similar to the initial binding pose (Figures 5A and S19B). In addition, we simulated the interaction of compound **7** with the E1-E2 complex and the details of the interaction pattern are described in Figure S23.

The most relevant interactions of **11** with E1-E2 included two hydrogen bonds, one between the NH_2^+ of the aminopyrimidine group and the side chain of E2-H29 and the other one between the OH group of the ligand and the amide of E1-V229 (Figure S21). Also, the phenoxy group established π - π interactions with E2-H29 and E2-H18 (Figure S22) and compound **11** had close hydrophobic contacts with E2-L16, E2-V242, E2-P243, and E1-M88. All these interactions remained stable for two replicates during the last 230 ns of the simulation but were slightly different for replicate number two. This was associated with a higher flexibility of domain B of E2 and the fusion peptide in this replica (Figure S19C) and the displacement of E2-H29.

The study of the mechanism of action of compound **11** suggested that binding of compound **11** to the E1-E2 complex occurs during internalization, *i.e.*, transit through the endocytic pathway. To study the likely interaction of compound **11** and the envelope protein complex in the acidic environment of the endosome, we performed MD simulations at pH 5.5. The analysis showed that compound **11** remained bound to pocket A during the 200 ns of the simulation (Figure S24).

To gain more insight into the energetics of the interaction between **11** and E1-E2, we performed MM-PBSA calculations^{22,23} with frames sampled from the last 230 ns of each simulation. We calculated the total binding energy and the contribution of the different amino acids to the interaction (Figure 5B). The total binding energy for the three replicates of compound **11** was -26 ± 3 kcal/mol. The residues with the larger contribution to the binding energy were E2-H29 and E1-M88, which is in agreement with the interactions described above. Mainly due to the positive net charge of the ligand, all nearby charged residues contributed in the same manner, with an attractive interaction for negatively charged residues and a repulsive interaction for positively charged ones (Figure S20). In turn, E2-P173S showed a modest contribution to binding of **11** and simulations done in the E2-P173S mutant showed a similar binding pattern to wild type. These results are in line with our observation that the E2-P173S mutant did not show resistance to the antiviral activity of compound **11** and has an effect only in combination with E1-Y24H.

Table 3. Experimental Solubility and Stability for Compound 11

compd	solubility (mM) ^a			stability [$t_{1/2}$ (min)] ^a				
	SGF ^b	SIF ^c	PBS ^d	SGF ^b	SIF ^c	PBS ^d	mouse plasma	human plasma
11	2.5 ± 0.8	2.7 ± 0.8	2.3 ± 0.4	>120	>120	>120	>120	>120

^aValues are expressed as the mean ± standard deviation of three independent experiments run in triplicate. ^bSimulated gastric fluid (pH 1.2). ^cSimulated intestinal fluid (pH 6.8). ^dPhosphate buffered saline solution (pH 7.4). United States Pharmacopeia (USP 23) solubility definition for M = 400 in water: 250 to 80 mM (soluble); 80 to 25 mM (sparingly soluble); 25 to 2.5 mM (slightly soluble); 2.5 to 0.25 mM (very slightly soluble); < 0.25 mM (practically insoluble).²⁹

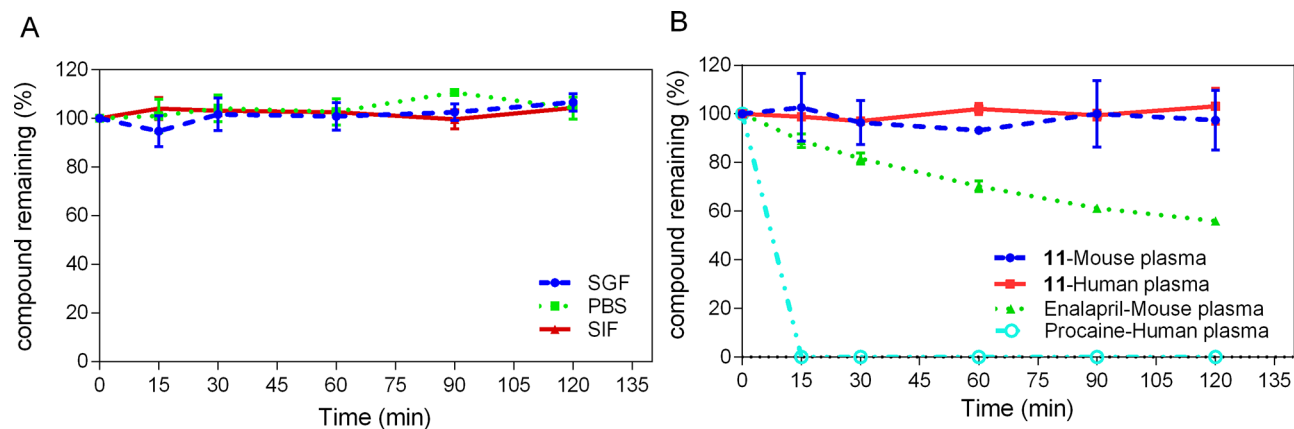


Figure 6. Experimental stability for compound 11. (A) Stability profile of 11 in SGF, SIF, and PBS. (B) Stability profile of 11 and enalapril in mouse plasma and 11 and procaine in human plasma. Compound remaining (%) quantification was based on the percentage relationship between the peak area of 11 at the test time and at $t = 0$ min. The peak area of 11 at $t = 0$ min was considered 100%. The values represent the mean percentage remaining against time with the error bars representing the standard deviation of three independent experiments.

Altogether, using MD simulations, we described a possible interaction pattern of compound 11 and the E1-E2 dimer that could be useful for the further optimization of these series of molecules or for the validation of the binding site of the compound.

Compound 11 Presents an Acceptable Solubility and Is Chemically and Enzymatically Stable. The efficacy and safety of molecules are highly interlinked with their ADME properties. An orally administered drug may only reach its target if it is well absorbed, distributed to the target site, and not cleared too rapidly from the body. The “drug-likeness” of a molecule is dependent on its physicochemical and structural properties. In particular, drug solubility is considered a fundamental property that has to be evaluated in the early stages of drug discovery. The current “gold-standard” shake-flask method was employed to study the solubility in three different media (simulated gastric fluid (SGF, pH 1.2), simulated intestinal fluid (SIF, pH 6.8) and phosphate buffered saline solution (PBS, pH 7.4)) of the most promising compound (11).^{24–27} The results are summarized in Table 3. Although the values observed indicate that 11 is only slightly soluble in all of the evaluated media, these are within the range usually observed for oral drugs.²⁸ Moreover, compounds designed for oral administration must be enzymatically and chemically stable at the low pH values observed in the stomach. To evaluate the stability of 11, the percentage of remaining drug after contact with SIF, SGH, PBS, and mouse and human plasma for 120 min was determined by HPLC-MS. Figure 6 shows that no modification or degradation of 11 was detected under the different investigated conditions. 11 had a high stability profile and half-life times ($t_{1/2}$) greater than 120 min. Figure 6B also presents the stability profiles obtained for the positive controls used for mouse and human plasma

(enalapril and procaine, respectively). Altogether, our results suggest that compound 11 should maintain a therapeutically effective formulation and no intrinsic instability and/or toxic degradation product issues should be expected.

DISCUSSION

Targeting of virus envelope proteins represents an attractive approach for development of antiviral strategies, as it implicates inhibition of the multistep virus entry process including virus–receptor interaction and internalization that involves envelope protein conformational rearrangement and subsequent virus–host membrane fusion. Yet, the discovery of small molecules that bind virus envelope proteins inhibiting their function has remained challenging. In this study, we used computer-aided drug design to identify ligands of the CHIKV E2-E1 envelope protein complex. Due to the lack of structural information on drug–protein interactions for CHIKV envelope proteins, we first aimed at identifying a druggable site. We chose a pocket relevant to the function of the CHIKV envelope protein complex (pocket A) that lies behind the fusion loop in E1 and in the interface between domain A and the β -ribbon and domain B of E2.⁴ A site analogue to pocket A has been previously used as the target for virtual screening leading to the identification of a series of hits including compound 7, although none of these hits were tested for antiviral activity.¹² Interestingly, compound 7 was the only hit identified in our virtual screening approaches displaying antiviral activity, and structure optimization led to the synthesis of compound 11, which showed an increase in antiviral potency compared to compound 7, and selectivity against CHIKV in cell culture.

In agreement with the selection of pocket A as a target, our characterization of the mode of action of compound 11

indicated that it is inhibiting virus entry at the step of internalization. Given the location of pocket A (Figure 1A), we speculate that the compound may be inhibiting the low-pH triggered conformational rearrangement of the envelope proteins and the membrane fusion process. The first step in the conformational rearrangement is the opening of domain B out of the fusion loop and domain A. An organic molecule binding into pocket A may stabilize the protein or disrupt the movement of domain B and therefore prevent the fusion process. To our knowledge, there is no inhibitor described so far with this mechanism of action for CHIKV or for any other alphavirus.

As an approach to validate the molecular target of compound **11**, we selected a CHIKV population resistant to the antiviral effect of the compound in cell culture. Two residue changes in E2 (S61R and P173S) and one in E1 (Y24H) dominated the population of drug-resistant viruses. E2-P173S is located in the back of pocket A (Figure 4D) in a hydrophobic region and E1-Y24 is located in the linker region between domains I and III of E1. Although separately none of the mutations conferred resistance to compound **11**, the E2-P173S E1-Y24H double mutant did show partial resistance to the antiviral activity of the compound. Interestingly, a functional link between E1 domain I and III linker and the region near the fusion loop has been reported.²⁰ The study describes the emergence of secondary mutations near the linker region of E1 following a systematic screen of substitution at residue E1-V80. As E1-V80 is implicated in the regulation of the fusion dynamics, the authors suggest that these two regions may coordinately regulate the fusion process. Moreover, Zheng et al. showed that the linker between domains I and III plays an important role in the conformational rearrangement of alphavirus envelope proteins that drive the fusion process.³⁰ In light of these results, we hypothesize that both mutations may be acting together in the regulation of E1-E2 function and further study of the single and double mutants biology may provide more evidence for the functional link between these distant regions of E1-E2 heterodimer. Moreover, the emergence of mutations in the envelope proteins that confer resistance to the antiviral activity of compound **11** supports our initial approach, suggesting that the envelope proteins are likely the target of compound **11**. Further work is needed to pinpoint the target site to pocket A. In this regard, the results obtained with the MMPBSA calculations of the molecular dynamics simulation suggest that residues E2-H29 and E1-M88 establish the most relevant interactions contributing to the binding energy of **11** with the E1-E2 dimer. It would be interesting to assess whether mutation of these two residues has an impact on the antiviral activity of compound **11** as an alternative approach to validate the molecular target of the compound. These calculations also support the selection of E2-P173S in the resistant virus population. However, the modest contribution of E2-P173 to the binding energy of **11** provides a plausible explanation to the drug-sensitive phenotype of the single mutant virus. As E1-Y24H is sensitive to **11** as well, we speculate that E1-Y24H has an allosteric effect on compound binding to pocket A, thus explaining why E2-P173S and E1-Y24H were combined in the adapted virus population.

Finally, mutations in an exposed region of E2 domain A arise in both antiviral resistant (E2-S61R) and cell culture adapted (E2-D63G) virus populations. Different mutations in this region have been implicated in the adaptation of alphaviruses to cell culture passaging and were linked to the use of the

abundantly expressed sulfated proteoglycans for attachment to the surface of BHK-21 and Vero cells. For instance, E2-Q55H and E2-E70K were found to increase SINV binding to heparan sulfate.^{31,32} These mutations, in the same way as E2-S61R, involve the gain of a positively charged amino acid. In turn, similar to the case of E2-D63G, E2-D60G occurred in a cell culture adapted CHIKV strain and results in the loss of negative charge that would have the effect of increasing binding to negatively charged proteoglycans.³³

All in all, the activity of compound **11** in the early stages of the viral life cycle, presumably inhibiting a direct viral target during virus entry, and the emergence of mutations in the envelope proteins associated with resistance to the antiviral activity of the compound serve as an initial validation to the selection of E1-E2 for the design of antiviral molecules. Furthermore, the linkage between distant residues, E2-P173 and E1-Y24, raises interesting implications about the function of CHIKV envelope proteins that warrant further investigation. Further work is needed to narrow down the target site of compound **11** to pocket A. The contribution of the binding energy of different amino acids obtained from molecular dynamics simulations may provide valuable insights in this regard or for further optimization of compound **11** derivatives. Finally, the adequate solubility and stability profile of compound **11** make this molecule a promising starting point for the development of CHIKV antivirals.

CONCLUSION

Based on computer-aided drug design, we selected a suitable pocket for antiviral targeting of CHIKV E1-E2 complex. Through the virtual screening of 915 000 molecules in pocket A using three different docking software, we selected seven compounds based on the consensus scoring, scaffold diversity, drug-like properties and synthetic feasibility for further modifications. One of the selected compounds (compound **7**) showed antiviral activity in cell-based assays and compound **11** emerged from lead optimization strategies and demonstrated to inhibit virus entry at the step of internalization. Mutations on E1-E2 associated with antiviral resistance to compound **11** provided pharmacological evidence for the rational design and optimization of lead molecules targeting CHIKV envelope glycoprotein complex. Moreover, compound **11** showed adequate solubility and stability on different media in addition to its antiviral activity, encouraging further optimization of this series of molecules for the development of CHIKV antivirals.

METHODS

Computational Chemistry. Protein System Preparation.

All simulations were based on the crystal structure of the ectodomain of the mature envelope proteins of CHIKV (PDB 3N42).⁴ E3 was removed from the protein complex, as evidence suggests that it is released after CHIKV maturation.³⁴ The protein was prepared for docking using the dockPrep tool of USFC Chimera.³⁵ Briefly, water and ion molecules were removed, and only highest occupancy of alternate locations of side chains were kept and hydrogens were added. All lysines and arginines were considered positively charged, and glutamates and aspartates negatively charged. The protonation state of histidines was determined taking into account the hydrogen bond network, and histidines near the binding pocket were visually inspected. ADT¹⁷ was used to assign

Gasteiger partial charges to every atom and to convert the protein to PDBQT file used for docking with AutoDock Vina¹⁵ and AutoDock4.¹⁷ For docking with LeDock, the protein was prepared with LePro.¹⁸

Binding Site Identification. To identify binding sites in the envelope proteins of CHIKV we compared the results of three different software, FPocket,³⁶ SiteHound³⁷ and P2Rank.³⁸ These software search for binding sites on the protein surface using different approaches. FPocket uses a geometric algorithm based on Voronoi tessellation to detect cavities in the protein surface, SiteHound is an energetic method, it detects binding pockets by placing a probe around the protein and calculating the molecular interaction energy and P2Rank is a machine learning algorithm. All programs were used with default parameters. The probe used for SiteHound was CMET.

Compound Library Preparation. Chembridge (https://www.chembridge.com/screening_libraries/diversity_libraries/) and NCI (<https://dtp.cancer.gov/>) databases were used. The structural similarity (Tanimoto coefficient > 0.7), mutagenicity and tumorigenicity risks for each compound were predicted with DataWarrior.³⁹ All compounds with high mutagenic or tumorigenic risk were discarded. Also, molecules that violated the Veber rule⁴⁰ were discarded and only compounds with no more than one violation to the Lipinski rule of five⁴¹ were admitted. The filtered molecules were prepared for docking with OpenBabel.⁴² After removing the salts, molecules were protonated at pH 7, a Gasteiger partial charge was assigned to every atom and a 3D conformer of the molecule was generated and minimized.

High throughput Docking. Docking was performed within pocket A with AutoDock Vina,¹⁵ LeDock¹⁸ and AutoDock4.¹⁷ The receptor was considered rigid. The search space was defined following the guidelines outlined by Trott et al.¹⁵ The search space was centered at X: -39.59, Y: -32.94, Z: -24.38, and the box dimensions were 27.5, 22.5, and 22.5 Å for XYZ respectively. For all docking programs, we used the default parameters. First compound libraries were docked with AutoDock Vina and all molecules that did not enter into the binding pocket were discarded. Filter molecules were docked with LeDock and AutoDock4 and were ranked by the exponential consensus ranking.¹⁸ Final molecules were selected by visual inspection of the top ranked molecules, considering the overall 3D conformation, the scaffold diversity and the synthetic tractability for potential modifications.

Molecular Dynamics and MM PBSA Calculations. In order to describe the possible interactions of compound 11 with E1-E2 we performed molecular dynamic simulations (MD) of the ligand protein complex. We used a reduced model of E1-E2 to reduce the computational cost (Figure S18). All simulations were done using GROMACS 5.0.7 software package.⁴³ As an initial configuration of the system, we used the ligand protein complex obtained after docking. The protonation state of all titratable residues was defined using PROPKA.^{44,45} We used the Amber99SB*-ILDN^{46,47} force field for the protein. We parametrized compound 11 using ANTECHAMBER with the GAFF2 force field,⁴⁸ and we converted the obtained topology and parameters to GROMACS compatible files with ACPYPE.⁴⁹ We used a 10 Å cutoff for nonbonded interactions, and long-range electrostatics was treated with PME. The system was solvated in a triclinic box of TIP3P⁵⁰ water extending 12 Å from the protein and was neutralized with 0.15 M NaCl. To remove steric clashes, the system was minimized for 50 000 steps with Steepest Descent algorithm and then was

heated to 310 K. The system was equilibrated for 200 ps in the NVT ensemble using the V-rescale thermostat⁵¹ with a coupling constant of 0.1 ps and for 1 ns in the NPT ensemble using the Berendsen pressure coupling algorithm⁵² with a reference pressure of 1 bar and a coupling constant of 2 ps. In all the equilibration phases, a position restrain (1000 kJ mol⁻¹ nm⁻²) was applied to all the heavy atoms of the ligand and protein. Finally, a 250 ns production run was performed on the NPT ensemble using the V-rescale thermostat and the Parrinello–Rahman barostat.⁵³ The first 20 ns of the simulation was not considered for analysis. To maintain the stability of the model during the simulation, we applied distance dependent position restraints in backbone atoms within 10 Å of the interface between the model and the rest of the viral spike and in all heavy atoms within 5 Å of the interface (Figure S18). For the equilibration and production runs, we used the LINCS constraint-algorithm⁵⁴ allowing a 2 fs time step.

For the analysis of MD trajectories, we used GROMACS tools and VMD.⁵⁵ For the MM-PBSA calculations, we used *g_mmpbsa*.²² We did the calculations with 460 water stripped frames sampled from the last 230 ns of each MD run. With the exception of the protein dielectric constant (6), we used all default parameters. We calculated the total binding energy and the contribution to the binding energy of each residue. All molecular modeling images were done with VMD.

Chemistry. General Information. All reagents and solvents were obtained from commercial sources, and compounds 1–6 were obtained from Molport. Column chromatography was carried out employing Merck silica gel (Kieselgel 60, 63–200 m). Precoated silica gel plates F-254 were used for thin-layer analytical chromatography. Structural analysis by ¹H NMR and ¹³C NMR confirmed the identity of compounds and synthesis intermediates, and mass spectrometry was used to determine their exact mass. NMR spectra were recorded on Bruker Advance II 500 MHz spectrometers at room temperature. Chemical shifts (δ) are reported in ppm, and coupling constants (J) are reported in Hertz. The mass spectrometer utilized was a Xevo G2S QTOF (Waters Corporation, Manchester, UK) with an electrospray ionization (ESI) source. It was operated in positive and negative ion modes with probe capillary voltages of 2.5 and 2.3 kV, respectively. The sampling cone voltage was 30 V. The source and desolvation gas temperatures were set to 120 and 350 °C, respectively. The nitrogen gas desolvation flow rate was 600 L h⁻¹, and the cone desolvation flow rate was 10 L h⁻¹. The mass spectrometer was calibrated across the range of m/z 50–1200 using a 0.5 mM sodium formate solution prepared in 2-propanol/water (90:10 v/v). Data was drift corrected during acquisition using a leucine enkephalin reference spray (LockSpray) infused at 2 μ L min⁻¹. Data was acquired in the range of m/z 50–1200, and the scan time was set from 22 to 1 s. Data acquisition and processing were carried out using MassLynx, ver. 4.1 (Waters Corp., Milford, MA, USA).

General Procedure for the Synthesis of Epoxides. Aqueous NaOH (1 M, 4 mL, 4.3 mmol) was added to a solution of phenol (400.0 mg, 4.3 mmol) or 4-methylphenol (465.0, 4.3 mmol) in THF (0.8 mL). After stirring for 15 min at room temperature, epichlorohydrin (663.0 μ L, 8.6 mmol) was added dropwise. The mixture was stirred at room temperature for 5 days. The epichlorohydrin excess and THF were removed on a rotary evaporator, and 1 M aqueous NaOH (5.0 mL) was added. The aqueous residue was extracted with AcOEt (3 \times 10

mL). Then, the combined organic phases were washed with 1 M aqueous NaOH (1 × 10 mL) and water (1 × 10 mL), dried over Na₂SO₄, and filtered, and the solvent was removed under reduced pressure. The resulting oil was purified via silica gel chromatography (cyclohexane/AcOEt 9:1) to obtain the desired epoxide as a syrup.

Phenyl Glycidyl Ether (8). Yield: (387.2 g, 60%). ¹H NMR (500 MHz, CDCl₃) δ 7.29 (dd, *J* = 1.1, 8.8 Hz, 2H), 6.97 (tt, *J* = 1.1, 7.5 Hz, 1H), 6.93 (dd, *J* = 7.5, 8.8 Hz, 2H), 4.22 (dd, *J* = 3.3, 11.0 Hz, 1H), 3.98 (dd, *J* = 5.6, 11.0 Hz, 1H), 3.38–3.35 (m, 1H), 2.91 (dd, *J* = 4.2, 4.9 Hz, 1H), 2.77 (dd, *J* = 2.7, 4.9 Hz, 1H). ¹³C NMR (125.7 MHz, CDCl₃) δ 158.6, 129.6, 121.4, 114.8, 68.8, 50.3, 44.9.

4-Methylphenylglycidyl Ether (9). Yield: (458.9 g, 65%). ¹H NMR (500 MHz, CDCl₃) δ 7.09 (dd, *J* = 8.5 Hz, 2H), 6.83 (dd, *J* = 8.5 Hz, 2H), 4.18 (dd, *J* = 3.3, 11.0 Hz, 1H), 3.92 (dd, *J* = 5.6, 11.0 Hz, 1H), 3.35–3.33 (m, 1H), 2.90 (br t, *J* = 4.6 Hz, 1H), 2.75 (dd, *J* = 2.6, 4.9 Hz, 1H), 2.29 (s, 3H). ¹³C NMR (125.7 MHz, CDCl₃) δ 156.5, 130.6, 130.1, 114.7, 68.9, 50.3, 44.9, 20.6.

General Procedure for the Synthesis of β-Amino Alcohols. The appropriate epoxide (0.3–0.7 mmol, 1.0 equiv) was dissolved in MeOH (1.5–3.0 mL, 0.17 M), and the respective amine (0.3–0.7 mmol, 1.5 equiv) was added. The mixture was stirred at room temperature for 48 h. Solvent was removed on a rotary evaporator, and then the residue was dissolved in CH₂Cl₂ and washed with distilled water. The organic layer was dried with Na₂SO₄, filtered, and evaporated under vacuum. The products were obtained after purification by recrystallization or silica gel chromatography.

1-(4-Methylphenoxy)-3-[4-(4-methylphenyl)piperazin-1-yl]propan-2-ol (7). Compound 7 was prepared from 4-methylphenyl glycidyl ether (50.0 mg, 0.30 mmol) and 1-(4-methylphenyl)piperazine (53.7 mg, 0.30 mmol) and was recrystallized from EtOH as a white solid (59.9 mg, 0.16 mmol, 53%). ¹H NMR (500 MHz, CDCl₃) δ 7.09–7.08 (m, 4H), 6.87–6.82 (m, 4H), 4.16–4.11 (m, 1H), 4.01 (dd, *J* = 5.7, 9.8 Hz, 1H), 3.98 (dd, *J* = 4.9, 9.8 Hz, 1H), 3.21–3.13 (m, 4H), 2.86–2.82 (m, 2H), 2.64–2.57 (m, 4H), 2.29 (s, 3H), 2.28 (s, 3H). ¹³C NMR (125.7 MHz, CDCl₃) δ 156.8, 149.2, 130.4, 130.0, 129.8, 129.5, 116.6, 114.6, 70.5, 65.8, 60.7, 53.5, 50.0, 20.6 (2C). HRMS (ESI-Q-ToF, *m/z*): [M + H]⁺ calcd for [C₂₁H₂₉N₂O₂]⁺ 341.2224; found: 341.2236; [M + Na]⁺ calcd for [C₂₁H₂₈N₂O₂Na]⁺ 363.2043; found: 363.2052

1-[4-(3-Chlorobenzyl)piperazin-1-yl]-3-(4-methylphenoxy)propan-2-ol (10). Compound 10 was prepared from 4-methylphenyl glycidyl ether (50.0 mg, 0.30 mmol) and 1-(3-chlorobenzyl)piperazine (56.7 μL, 0.30 mmol) and recrystallized from EtOH/H₂O as a white solid (50.0 mg, 0.13 mmol, 43%). ¹H NMR (500 MHz, CDCl₃) δ 7.34 (br t, *J* = 7.6, 8.7 Hz, 1H), 7.24–7.18 (m, 3H), 7.07 (d, *J* = 8.4 Hz, 2H), 6.82 (d, *J* = 8.4 Hz, 2H), 4.09–4.05 (m, 1H), 3.97–3.92 (m, 2H), 3.48 (s, 2H), 2.70 (br s, 2H), 2.59–2.49 (m, 8H), 2.28 (s, 3H). ¹³C NMR (125.7 MHz, CDCl₃) δ 156.8, 140.5, 134.3, 130.3, 130.0, 129.6, 129.2, 127.4, 127.3, 114.6, 70.5, 65.7, 62.5, 60.6, 53.4, 53.3, 20.6. HRMS (ESI-Q-ToF, *m/z*): [M + H]⁺ calcd for [C₂₁H₂₈ClN₂O₂]⁺ 375.1834; found: 375.1842; [M + Na]⁺ calcd for [C₂₁H₂₇ClN₂O₂Na]⁺ 397.1653; found: 397.1657.

1-[(1-Benzylpiperidin-4-yl)amino]-3-phenoxypropan-2-ol (11). Compound 11 was prepared from phenyl glycidyl ether (100.0 mg, 0.66 mmol) and 4-amino-1-benzylpiperidine (134.5 μL, 0.66 mmol). The product was obtained after

purification by silica gel chromatography (CH₂Cl₂/MeOH 9:1) as a white solid (78.3 mg, 0.23 mmol, 35%). ¹H NMR (500 MHz, CDCl₃) δ 7.32–7.24 (m, 7H), 6.96 (br t, *J* = 7.34 Hz, 1H), 6.92 (br d, *J* = 8.41 Hz, 2H), 4.02–3.94 (m, 3H), 3.50 (s, 2H), 2.92 (dd, *J* = 3.2, 11.9 Hz, 1H), 2.85 (br dt, 2H), 2.76 (dd, *J* = 6.7, 11.9 Hz, 1H), 2.48 (tt, *J* = 4.0, 10.3 Hz, 1H), 2.02 (br t, *J* = 11.43 Hz, 2H), 1.89–1.86 (m, 2H), 1.45–1.36 (m, 2H). ¹³C NMR (125.7 MHz, CDCl₃) δ 158.8, 138.6, 129.6, 129.2, 128.3, 127.1, 121.1, 114.7, 70.5, 68.6, 63.2, 55.1, 52.5, 48.9. HRMS (ESI-Q-ToF, *m/z*): [M + H]⁺ calcd for [C₂₁H₂₉N₂O₂]⁺ 341.2224; found: 341.2236; [M + Na]⁺ calcd for [C₂₁H₂₈N₂O₂Na]⁺ 363.2043; found: 363.2052.

1-(4-Methylpiperazin-1-yl)-3-phenoxypropan-2-ol (12). Compound 12 was prepared from phenyl glycidyl ether (100.0 mg, 0.67 mmol) and 1-methylpiperazine (73.9 μL, 0.67 mmol). The product was obtained after purification by silica gel chromatography (CH₂Cl₂/MeOH 9:1) as a white solid (64.6 mg, 0.26 mmol, 39%). ¹H NMR (500 MHz, CDCl₃) δ 7.29–7.26 (m, 2H), 6.96–6.91 (m, 3H), 4.12–4.07 (m, 1H), 3.99 (m, *J* = 5.2, 9.8 Hz, 1H), 3.99 (m, *J* = 4.9, 9.8 Hz, 1H), 2.72 (br s, 2H), 2.60–2.49 (m, 8H), 2.30 (s, 3H). ¹³C NMR (125.7 MHz, CDCl₃) δ 158.8, 129.6, 121.1, 114.7, 70.3, 65.6, 60.6, 55.3, 53.4, 46.7. HRMS (ESI-Q-ToF, *m/z*): [M + H]⁺ calcd for [C₁₄H₂₃N₂O₂]⁺ 251.1754; found: 251.1773; [M + Na]⁺ calcd for [C₁₄H₂₂N₂O₂Na]⁺ 273.1573; found: 273.1591.

1-[(1,1'-Biphenyl)-4-ylamino]-3-phenoxypropan-2-ol (13). Compound 13 was prepared from phenyl glycidyl ether (50.0 mg, 0.33 mmol) and 4-biphenylamine (56.3 mg, 0.33 mmol) and recrystallized from MeOH as a white solid (20.6 mg, 0.07 mmol, 20%). ¹H NMR (500 MHz, CDCl₃) δ 7.54 (d, *J* = 7.4 Hz, 2H), 7.47 (d, *J* = 8.6 Hz, 2H), 7.39 (t, *J* = 7.6 Hz, 2H), 7.31 (dd, *J* = 7.6, 8.2 Hz, 2H), 7.27 (t, *J* = 7.4 Hz, 1H), 7.0 (d, *J* = 7.4 Hz, 1H), 6.94 (d, *J* = 8.2 Hz, 2H), 6.76 (d, *J* = 8.6 Hz, 2H), 4.32–4.28 (m, 1H), 4.12 (dd, *J* = 4.0, 9.4 Hz, 1H), 4.08 (dd, *J* = 6.2, 9.4 Hz), 3.50 (dd, *J* = 4.4, 13.0 Hz, 1H), 3.36 (dd, *J* = 7.1, 13.0 Hz, 1H). ¹³C NMR (125.7 MHz, CDCl₃) δ 158.5, 147.6, 141.3, 131.1, 129.7, 128.8, 128.2, 126.5, 126.3, 121.5, 114.7, 113.7, 70.1, 69.0, 46.7. HRMS (ESI-Q-ToF, *m/z*): [M + H]⁺ calcd for [C₂₁H₂₂NO₂]⁺ 320.1645; found: 320.1653; [M + Na]⁺ calcd for [C₂₁H₂₁NO₂Na]⁺ 342.1465; found: 342.1469.

Cells and Viruses. All cell lines were grown at 37 °C in a 5% CO₂ atmosphere. Vero cells (*Cercopithecus aethiops* kidney, ATCC CCL-81) were grown in Dulbecco's modified Eagle's medium (DMEM) supplemented with 10% fetal bovine serum (FBS) and penicillin–streptomycin antibiotics. For infections, Vero cells were cultured in DMEM supplemented with 2% FBS. BHK cells (*Mesocricetus auratus* hamster kidney, ATCC, CCL-10) were grown in MEM alpha medium supplemented with 10% FBS and antibiotics.

CHIKV-LR⁵⁶ and CHIKV-ZsGreen²⁰ were derived from infectious cDNA clones. For RNA synthesis, cDNAs were linearized by digestion with NotI and used as templates for transcription by SP6 polymerase in the presence of the GpppG cap structure analogue, using the mMessage mMachine transcription kit (Thermo Fisher) according to the manufacturer's instructions. BHK cells were transfected with *in vitro* transcribed RNA using Lipofectamine 2000 (Invitrogen) following the manufacturer's instructions. Virus in the supernatant was harvested 48 h later and amplified once in Vero cells. Viral titers of the final stocks were determined by plaque assay. Viral stocks were stored at –70 °C until use.

Viral Titer Determination by Plaque Assay. Approximately 10^5 Vero cells per well were seeded in 24-well plates and were allowed to attach overnight. Cells were infected with serial dilutions of viral stocks. After 1 h of incubation at 37 °C, 1 mL of overlay (1× DMEM medium, 2% FBS, 100 U of penicillin/mL, and 0.4% methylcellulose) was added to each well. Cells were fixed 3 days post infection with 10% formaldehyde and stained with crystal violet (20% ethanol, 0.1% crystal violet) to allow plate lysis count.

Cytotoxicity Assay. To determine the cytotoxic effect of the compounds, 10^4 Vero cells per well were seeded in 96-well plates and were allowed to attach overnight. Cells were treated in quadruplicate with serial dilutions of each compound or with 1% DMSO as a control and were incubated at 37 °C for 3 days. Cell viability was determined via MTT (3-(4,5-dimethylthiazol-2-yl)-2,5-diphenyltetrazolium bromide) assay. Cells were washed twice with PBS and incubated with DMEM 2% FBS and MTT at a final concentration of 0.5 mg/mL for 4 h at 37 °C. Afterward, blue precipitates were dissolved for 1 h at 37 °C in 0.1 mL of isopropanol/HCL (300:1). Finally, the absorbance at 570 nm was recorded in a spectrophotometer. The absorbance value from blank wells containing only medium and reagents was subtracted from all the samples and the percentage of viability for each treatment was determined in comparison to DMSO control. The cytotoxic concentration 50 (CC_{50}) was determined with a nonlinear curve fit of the viability data obtained from the average of three independent experiments.

Antiviral Activity Determination by Flow Cytometry. To determine the antiviral activity of compounds, approximately 10^5 Vero cells per well were seeded in 24-well plates and were allowed to attach overnight. Cells were treated in duplicate with serial dilutions of each compound or with DMSO control and were infected with 10^3 PFU of CHIKV-ZsGreen. After 1 h of incubation at 37 °C, cells were overlaid with the corresponding concentration of each compound in culture media and were incubated at 37 °C for 24 h. The percentage of infected cells was determined by flow cytometry. Cells were washed with PBS, lifted with trypsin 0.05%, and fixed with PFA 4%. The fluorescence signal was measured using a flow cytometer (CyFlow Space, Partec) at a detection spectrum of 488 nm. The percentage of infected cells was determined using two sequential gatings, with the first one in the FSC-SSC space to select the cell population and the second one in the FL1 histogram to differentiate infected cells from noninfected cells. Both gatings were defined in the uninfected control. Data analysis was done with the FlowJo 7.6.2 software package. The percentage of inhibition for each compound concentration was calculated from the relative infection of each treatment in comparison to the level of infection in the DMSO control. The EC_{50} of each compound was determined from the non linear fit of the inhibition data obtained from three independent experiments.

Time of Drug Addition Assay. Approximately 10^5 Vero cells per well were seeded in 24-wells plates and were allowed to attach overnight. Cells were infected with CHIKV-ZsGreen with a MOI of 0.1 and treated with 30 μ M of compound **11** at different time points during or after the infection. For the treatment during the infection, cells were simultaneously treated with **11** and infected with CHIKV-ZsGreen. For the rest of the treatments, cells were infected in the absence of drug. After 1 h of incubation at 37 °C, the inoculum was removed and cells were washed twice with PBS to remove

noninternalized virus. For the cotreatment and the treatment at 1 h post infection, cells were covered with 30 μ M **11** in culture media. For the rest of the treatments and nontreated control, cells were covered with culture media and compound **11** was added at the corresponding time point after the infection. After 8 h of incubation at 37 °C, a fresh monolayer of Vero cells was infected with a 1:50 dilution of each supernatant. After this dilution, **11** is at a nonactive concentration. Cells were incubated for 2 days, and the percentage of infected cells was determined by flow cytometry.

Virucidal Activity Assay. CHIKV-ZsGreen (10^6 PFU/mL) was incubated with different concentrations of compound **11** in DMEM for 1 h at 37 °C. After the incubation, Vero cells grown overnight in 24-well plates were infected with a 1:100 dilution of the mixture. After this dilution, the compound is diluted to a nonactive concentration and the infection is at MOI 0.01. One day post infection, the percentage of infected cells was determined by flow cytometry and relativized to the nontreated control.

Attachment Assay. To determine the effect of compound **11** in CHIKV attachment, we used a previously published method with modifications.⁵⁷ Briefly, 2×10^5 Vero cells per well were seeded in 12-well plates and were allowed to attach overnight. Cells were simultaneously treated with 50 μ M compound **11** and infected with CHIKV-ZsGreen with a MOI of 0.1. After the incubation for 30 min at room temperature, cells were washed twice with PBS to remove nonattached virus and were harvested in culture media with a cell scraper. Cells were lysed by three freeze–thaw cycles, and the supernatant was clarified by centrifugation for 10 min at 1000g at 4 °C. A fresh monolayer of Vero cells was infected with the clarified supernatant, and after 2 days of incubation at 37 °C the percentage of infected cells was determined by flow cytometry.

Internalization Assay. To determine the effect of compound **11** in CHIKV internalization, we followed a previously described method with modifications.⁵⁷ Briefly, 10^5 Vero cells per well were seeded in 24-well plates and were allowed to attach overnight. Cells were infected with CHIKV-ZsGreen with a MOI of 0.1 and were incubated for 30 min at room temperature. Afterward, cells were washed twice with PBS to remove nonattached virus and were treated with 50 μ M of **11**. After 1 h of incubation at 37 °C, cells were washed with PBS and were treated for 10 min with 0.25% trypsin. Cells were harvested, and trypsin was inactivated with 2 mM PMSF. Finally, cells were washed with PBS and plated over a fresh monolayer of Vero cells. After 2 days of incubation, the percentage of infected cells was determined by flow cytometry.

Virus Selection by Serial Passaging in Cell Culture. Selection was performed in 24-well plates. For each passage, cells were infected with CHIKV-LR with a MOI of 0.01 in the presence of compound **11**. The concentration of **11** was gradually increased from 5 to 50 μ M in 14 passages. The virus population was harvested 2 or 3 days after the infection, when a significant cytopathic effect was observed, and the viral titer was determined by plaque assay. After 14 passages, the sensitivity to **11** was determined and the envelope region of CHIKV genome was sequenced. To this end, the RNA genome was Trizol-extracted from culture supernatants and used as a template for cDNA synthesis with primers 95 and 137. Products of reverse transcription were amplified by PCR with primers 95–93 and 137–136, correspondingly. PCR products were sequenced by the Sanger method using the

primers 93, 95, 136, and 137. Primer sequences and nucleotide positions are presented in Table S2.

Sensitivity of Adapted Virus Populations to Compound 11. Approximately 10^5 Vero cells per well were seeded in 24-wells plates and were allowed to attach overnight. Cells were treated with different concentrations of compound 11 and infected with viruses recovered after the 14th passage of the serial virus passage experiment at a MOI of 0.01 or with CHIKV-LR WT. After 24 h, cells were treated with 1 mM EDTA, harvested, and fixed with PFA 4%. Fixed cells were first incubated with a mouse antibody against E2 (Novus Biologicals, NBP2-53111) in FACS buffer (PBS 1% BSA 0.01% azide) and then with a secondary antibody conjugated to AlexaFluor 488 (Invitrogen). The percentage of E2 expressing cells was determined by flow cytometry as previously described. In independent experiments, the viral yield in the supernatant was determined by plaque assay at 48 h after the infection.

Construction of CHIKV-ZsGreen E1-Y24H, E2-P173S and E1-Y24H E2-P173S Double Mutant. E1-Y24 and E2-P173 were mutated to H and S, respectively, in the WT CHIKV-ZsGreen by overlapping PCR. The first PCR reactions were done with primers Fw173–137 and Rv173–164 for E2-P173S and with primers Fw24–92 and Rv24–165 for E1-Y24H mutant. Overlapping PCR products for each mutant were then amplified with primers 164–137 for E2-P173S and 165–92 for E1-Y24H. All PCR was done with AccuPrime Pfx DNA polymerase from ThermoFisher Scientific following the manufacturer's instructions. Obtained PCR products were cloned in CHIKV-ZsGreen infectious cDNA clones using SpeI and XhoI restriction enzymes for E2-P173S and XhoI and NotI for E1-Y24H. Individual clones were checked by Sanger sequencing to check for the insertion of the desired mutations and the absence of any additional mutation in DNA sequence. Viral stocks were produced from infectious cDNA clones following in vitro transcription and transfection.

Physical and Pharmacokinetics Properties. The buffer solutions used in the solubility test and stability assays (SIF, SGF, PBS) were prepared according to the specifications given in the United States Pharmacopeia (25th edition). In particular, SGF was prepared using NaCl and HCl and SIF using KH_2PO_4 and NaOH.

Shake-Flask Method for Drug Solubility Testing. The shake-flask method was used as a reference assay^{24–26} to test the solubility of 11 in simulated gastric fluid (SGF, pH 1.2), simulated intestinal fluid (SIF, pH 6.8), and phosphate buffered saline solution (PBS, pH 7.4). Briefly, 11 (1 mg) was weighted into a 2 mL glass vial, and 1 mL of the medium (SGF, SIF, or PBS) was added. Then, the suspension was mixed at 1500 rpm at 37 °C for 24 h and subsequently incubated at 37 °C for 24 h without stirring. Finally, the sample was filtered (0.2 mm Sterile Acrodisc 13, Gelman-Science), and the filtrate was diluted in MeOH/media (1:1). The solution concentration was determined by UV spectroscopy (Shimadzu 3600 UV/vis/NIR spectrophotometer). The calibration curve was obtained by serial dilution of the 11 stock solution (1 mg/mL, DMSO) in MeOH/media (1:1) and was constructed by plotting the absorbance of the compounds against the concentration. The compound was tested in triplicate in each medium.

SGF, SIF, PBS, and Mouse and Human Plasma Stability. Stability assays were performed for compound 11 according to the procedure described in a previous work.²⁵ Briefly, stock

solutions of 11 in DMSO (10 mM) were diluted to 1 mM (in acetonitrile for SGF, SIF, PBS and DMSO for mouse and human plasma). The stability assay reactions were initiated by the addition of 11 to the SGF, SIF, or PBS medium or to a preheated plasma solution (diluted to 80% with PBS). Samples (50 mM) were incubated in a shaking water bath at 37 °C and conducted in triplicate. Aliquots were taken at 0, 15, 30, 60, 90, and 120 min, and acetonitrile containing the internal standard (warfarin) was added to quench the reaction. The samples were vortexed and then centrifuged. The supernatant was collected, diluted in methanol/water (50:50), and analyzed by high performance liquid chromatography–mass spectrometry (HPLC-MS). The quantification was based on the peak area ratio of the test compound vs the internal standard. The HPLC-MS analysis was performed using a Waters Alliance e2695 system (Waters Corporation, Milford, MA, USA) fitted with a Phenomenex Kinetex XB-C18 (150 × 4.6 mm, 5 μm particle size, Phenomenex Inc., Torrance, CA, USA) coupled to a Waters SQD2 single quadrupole mass spectrometer with an electrospray ionization (ESI) source. Gradient elution was used in the chromatographic separation method using 40% water and 0.1% acetic acid (mobile phase A), 40% methanol (mobile phase B), with the following program: 0–3 min 40% B; 3–7 min 40–90% B; 7–20 min 90% B. The flow rate was constant at 0.35 mL min⁻¹. After each sample injection, the gradient was returned to its initial conditions in 16 min. The injection volume was 5 μL. The column temperature was 35 °C. The mass spectrometer was operated in positive ion mode with a probe capillary voltage of 2.5 kV. The sampling cone voltage was set to 35.0 V. The source and desolvation gas temperatures were set at 150 and 350 °C, respectively. The nitrogen gas desolvation flow rate was 600 L h⁻¹, and the cone gas flow rate was 10 L h⁻¹. The mass spectrometer was calibrated across the range of m/z 20–2023 with a sodium and cesium iodide solution. Data were acquired in the scan mode with a scan duration of 0.2 s and in the SIR mode with unit resolution. Data acquisition and processing were carried out using MassLynx, ver. 4.1 software. Enalapril and procaine were used as positive controls for mouse and human plasma, respectively.

Statistical Analysis. All statistical analysis and nonlinear curve fitting were done using GraphPad Prism 5 software.

■ ASSOCIATED CONTENT

Supporting Information

The Supporting Information is available free of charge at <https://pubs.acs.org/doi/10.1021/acsinfecdis.0c00915>.

¹H and ¹³C NMR and HMRS spectral charts for compounds 7 and 10–13; virtual screening workflow and results; molecular dynamics plots for compounds 7 and 11; total binding free energy MMPBSA method for compounds 1–7 and 11; primers used in this study (PDF)

■ AUTHOR INFORMATION

Corresponding Authors

Mariela Bollini – Laboratorio de Química Medicinal, Centro de Investigaciones en Bionanociencias (CIBION), Consejo Nacional de Investigaciones Científicas y Técnicas (CONICET), Ciudad Autónoma de Buenos Aires C1425FQD, Argentina; orcid.org/0000-0002-8718-6236; Email: mariela.bollini@cibion.conicet.gov.ar

Diego E. Álvarez – Instituto de Investigaciones Biotecnológicas, Consejo Nacional de Investigaciones Científicas y Técnicas (CONICET), Universidad Nacional de San Martín, San Martín B1650, Argentina; Email: dalvarez@iib.unsam.edu.ar

Authors

Leandro Battini – Laboratorio de Química Medicinal, Centro de Investigaciones en Bionanociencias (CIBION), Consejo Nacional de Investigaciones Científicas y Técnicas (CONICET), Ciudad Autónoma de Buenos Aires C1425FQD, Argentina; Instituto de Investigaciones Biotecnológicas, Consejo Nacional de Investigaciones Científicas y Técnicas (CONICET), Universidad Nacional de San Martín, San Martín B1650, Argentina

Daniela M. Fidalgo – Laboratorio de Química Medicinal, Centro de Investigaciones en Bionanociencias (CIBION), Consejo Nacional de Investigaciones Científicas y Técnicas (CONICET), Ciudad Autónoma de Buenos Aires C1425FQD, Argentina

Complete contact information is available at:

<https://pubs.acs.org/10.1021/acsinfectdis.0c00915>

Author Contributions

[§]D.E.A. and M.B. contributed equally. The manuscript was written through contributions of all authors.

Funding

This work was supported by the Agencia Nacional de Promoción Científica y Tecnológica, Argentina (PICT 2017–3767), Consejo Nacional de Investigaciones Científicas y Técnicas (CONICET) (PIP 2014 11220130100721).

Notes

The authors declare no competing financial interest.

ACKNOWLEDGMENTS

The authors thank María Eugenia Monge for her support in mass spectrometry. The authors also wish to thank Centro de Cálculo de Alto Desempeño (Universidad Nacional de Córdoba) and TUPAC Cluster from CSC–CONICET, which is part of SNCAD–MinCyT. CHIKV La Reunion infectious clone expressing ZsGreen was a kind gift of Kenneth A. Stapleford (Department of Microbiology, New York University School of Medicine).

REFERENCES

- <https://www.paho.org/data/index.php/en/mnu-topics/chikv-en>.
- Holmes, A. C., Basore, K., Fremont, D. H., and Diamond, M. S. (2020) A Molecular Understanding of Alphavirus Entry. *PLoS Pathog.* 16 (10), No. e1008876.
- Van Duijl-Richter, M. K. S., Hoornweg, T. E., Rodenhuis-Zybert, I. A., and Smit, J. M. (2015) Early Events in Chikungunya Virus Infection—From Virus CellBinding to Membrane Fusion. *Viruses* 7 (7), 3647–3674.
- Voss, J. E., Vaney, M.-C., Duquerooy, S., Vornrhein, C., Girard-Blanc, C., Crublet, E., Thompson, A., Bricogne, G., and Rey, F. A. (2010) Glycoprotein Organization of Chikungunya Virus Particles Revealed by X-Ray Crystallography. *Nature* 468 (7324), 709–712.
- Li, L., Jose, J., Xiang, Y., Kuhn, R. J., and Rossmann, M. G. (2010) Structural Changes of Envelope Proteins during Alphavirus Fusion. *Nature* 468 (7324), 705–708.
- Lu, L., Yu, F., Cai, L., K. Debnath, A., and Jiang, S. (2015) Development of Small-Molecule HIV Entry Inhibitors Specifically Targeting Gp120 or Gp41. *Curr. Top. Med. Chem.* 16, 1074–1090.
- Kovacikova, K., and van Hemert, M. J. (2020) Small-Molecule Inhibitors of Chikungunya Virus: Mechanisms of Action and Antiviral Drug Resistance. *Antimicrob. Agents Chemother.* 64 (12), e01788-20.
- Abdelnabi, R., Neyts, J., and Delang, L. (2016) Antiviral Strategies Against Chikungunya Virus. *Methods Mol. Biol.* 1426, 243–253.
- Ho, Y.-J., Wang, Y.-M., Lu, J., Wu, T.-Y., Lin, L.-I., Kuo, S.-C., and Lin, C.-C. (2015) Suramin Inhibits Chikungunya Virus Entry and Transmission. *PLoS One* 10 (7), No. e0133511.
- Albulescu, I. C., White-Scholten, L., Tas, A., Hoornweg, T. E., Ferla, S., Kovacikova, K., Smit, J. M., Brancale, A., Snijder, E. J., and van Hemert, M. J. (2020) Suramin Inhibits Chikungunya Virus Replication by Interacting with Virions and Blocking the Early Steps of Infection. *Viruses* 12 (3), 314.
- Agarwal, G., Gupta, S., Gabrani, R., Gupta, A., Chaudhary, V. K., and Gupta, V. (2019) Virtual Screening of Inhibitors against Envelope Glycoprotein of Chikungunya Virus: A Drug Repositioning Approach. *Bioinformation* 15 (6), 439–447.
- Rashad, A. A., and Keller, P. A. (2013) Structure Based Design towards the Identification of Novel Binding Sites and Inhibitors for the Chikungunya Virus Envelope Proteins. *J. Mol. Graphics Modell.* 44, 241–252.
- https://www.chembridge.com/screening_libraries/diversity_libraries/ (accessed 2018-03-10).
- <https://dtp.cancer.gov/> (accessed 2018-03-10).
- Trott, O., and Olson, A. J. (2010) AutoDock Vina: Improving the Speed and Accuracy of Docking with a New Scoring Function, Efficient Optimization, and Multithreading. *J. Comput. Chem.* 31 (2), 455–461.
- Zhang, N., and Zhao, H. (2016) Enriching Screening Libraries with Bioactive Fragment Space. *Bioorg. Med. Chem. Lett.* 26 (15), 3594–3597.
- Morris, G. M., Huey, R., Lindstrom, W., Sanner, M. F., Belew, R. K., Goodsell, D. S., and Olson, A. J. (2009) AutoDock4 and AutoDockTools4: Automated Docking with Selective Receptor Flexibility. *J. Comput. Chem.* 30 (16), 2785–2791.
- Palacio-Rodríguez, K., Lans, I., Cavasotto, C. N., and Cossio, P. (2019) Exponential Consensus Ranking Improves the Outcome in Docking and Receptor Ensemble Docking. *Sci. Rep.* 9 (1), 5142.
- <https://chemminetools.ucr.edu/> (accessed 2018-12).
- Noval, M. G., Rodriguez-Rodriguez, B. A., Rangel, M. V., and Stapleford, K. A. (2019) Evolution-Driven Attenuation of Alphaviruses Highlights Key Glycoprotein Determinants Regulating Viral Infectivity and Dissemination. *Cell Rep.* 28 (2), 460–471.
- Strauss, J. H., and Strauss, E. G. (1994) The Alphaviruses: Gene Expression, Replication, and Evolution. *Microbiol. Rev.* 58 (3), 491–562.
- Kumari, R., Kumar, R., and Lynn, A. (2014) G_mmpbsa—A GROMACS Tool for High-Throughput MM-PBSA Calculations. *J. Chem. Inf. Model.* 54 (7), 1951–1962.
- Baker, N. A., Sept, D., Joseph, S., Holst, M. J., and McCammon, J. A. (2001) Electrostatics of Nanosystems: Application to Microtubules and the Ribosome. *Proc. Natl. Acad. Sci. U. S. A.* 98 (18), 10037–10041.
- Bollini, M., Cisneros, J. A., Spasov, K. A., Anderson, K. S. K. S., and Jorgensen, W. L. (2013) Optimization of Diarylazines as Anti-HIV Agents with Dramatically Enhanced Solubility. *Bioorg. Med. Chem. Lett.* 23 (18), 5213–5216.
- Leal, E. S., Adler, N. S., Fernández, G. A., Gebhard, L. G., Battini, L., Aucar, M. G., Videla, M., Monge, M. E., Hernández de los Ríos, A., Acosta Dávila, J. A., Morell, M. L., Cordo, S. M., García, C. C., Gamarnik, A. V., Cavasotto, C. N., and Bollini, M. (2019) De Novo Design Approaches Targeting an Envelope Protein Pocket to Identify Small Molecules against Dengue Virus. *Eur. J. Med. Chem.* 182, 111628.
- Fernández, G. A., Castro, E. F., Rosas, R. A., Fidalgo, D. M., Adler, N. S., Battini, L., España de Marco, M. J., Fabiani, M., Bruno, A. M., Bollini, M., and Cavallaro, L. V. (2020) Design and Optimization

of Quinazoline Derivatives: New Non-Nucleoside Inhibitors of Bovine Viral Diarrhea Virus. *Front. Chem.* 8, 590235.

(27) Baka, E., Comer, J. E. A., and Takács-Novák, K. (2008) Study of Equilibrium Solubility Measurement by Saturation Shake-Flask Method Using Hydrochlorothiazide as Model Compound. *J. Pharm. Biomed. Anal.* 46 (2), 335–341.

(28) Frey, K. M. K. M., Puleo, D. E. D., Spasov, K. a., Bollini, M., Jorgensen, W. L., and Anderson, K. S. K. S. (2015) Structure-Based Evaluation of Non-Nucleoside Inhibitors with Improved Potency and Solubility That Target HIV Reverse Transcriptase Variants. *J. Med. Chem.* 58 (6), 2737.

(29) The United States Pharmacopeia, USP 23. The National Formulary, NF 18: Official from January 1, 1995; United States Pharmacopeial Convention, 1994.

(30) Zheng, Y., Sánchez-San Martín, C., Qin, Z., and Kielian, M. (2011) The Domain I-Domain III Linker Plays an Important Role in the Fusogenic Conformational Change of the Alphavirus Membrane Fusion Protein. *J. Virol.* 85 (13), 6334–6342.

(31) Smit, J. M., Waarts, B.-L., Kimata, K., Klimstra, W. B., Bittman, R., and Wilschut, J. (2002) Adaptation of Alphaviruses to Heparan Sulfate: Interaction of Sindbis and Semliki Forest Viruses with Liposomes Containing Lipid-Conjugated Heparin. *J. Virol.* 76 (20), 10128–10137.

(32) Levine, B., and Griffin, D. E. (1993) Molecular Analysis of Neurovirulent Strains of Sindbis Virus That Evolve during Persistent Infection of Scid Mice. *J. Virol.* 67 (11), 6872–6875.

(33) Tssetsarkin, K. A., McGee, C. E., Volk, S. M., Vanlandingham, D. L., Weaver, S. C., and Higgs, S. (2009) Epistatic Roles of E2 Glycoprotein Mutations in Adaption of Chikungunya Virus to Aedes Albopictus and Ae. Aegypti Mosquitoes. *PLoS One* 4 (8), No. e6835.

(34) Yap, M. L., Klose, T., Urakami, A., Hasan, S. S., Akahata, W., and Rossmann, M. G. (2017) Rossmann, M. G. Structural Studies of Chikungunya Virus Maturation. *Proc. Natl. Acad. Sci. U. S. A.* 114 (52), 13703–13707.

(35) Pettersen, E. F., Goddard, T. D., Huang, C. C., Couch, G. S., Greenblatt, D. M., Meng, E. C., and Ferrin, T. E. (2004) UCSF Chimera—a Visualization System for Exploratory Research and Analysis. *J. Comput. Chem.* 25 (13), 1605–1612.

(36) Le Guilloux, V., Schmidtke, P., and Tuffery, P. (2009) Fpocket: An Open Source Platform for Ligand Pocket Detection. *BMC Bioinf.* 10 (1), 168.

(37) Hernandez, M., Ghersi, D., and Sanchez, R. (2009) SITEHOUND-Web: A Server for Ligand Binding Site Identification in Protein Structures. *Nucleic Acids Res.* 37, W413–W416.

(38) Krivák, R., and Hoksza, D. (2018) P2Rank: Machine Learning Based Tool for Rapid and Accurate Prediction of Ligand Binding Sites from Protein Structure. *J. Cheminf.* 10 (1), 39.

(39) Sander, T., Freyss, J., von Korff, M., and Rufener, C. (2015) DataWarrior: An Open-Source Program For Chemistry Aware Data Visualization And Analysis. *J. Chem. Inf. Model.* 55 (2), 460–473.

(40) Veber, D. F., Johnson, S. R., Cheng, H.-Y., Smith, B. R., Ward, K. W., and Kopple, K. D. (2002) Molecular Properties That Influence the Oral Bioavailability of Drug Candidates. *J. Med. Chem.* 45 (12), 2615–2623.

(41) Lipinski, C. A., Lombardo, F., Dominy, B. W., and Feeney, P. J. (1997) Experimental and Computational Approaches to Estimate Solubility and Permeability in Drug Discovery and Development Settings. *Adv. Drug Delivery Rev.* 23 (1), 3–25.

(42) O'Boyle, N. M., Banck, M., James, C. A., Morley, C., Vandermeersch, T., and Hutchison, G. R. (2011) Open Babel: An Open Chemical Toolbox. *J. Cheminf.* 3 (1), 33.

(43) Abraham, M. J., Murtola, T., Schulz, R., Páll, S., Smith, J. C., Hess, B., and Lindahl, E. (2015) GROMACS: High Performance Molecular Simulations through Multi-Level Parallelism from Laptops to Supercomputers. *SoftwareX* 1–2, 19–25.

(44) Søndergaard, C. R., Olsson, M. H. M., Rostkowski, M., and Jensen, J. H. (2011) Improved Treatment of Ligands and Coupling Effects in Empirical Calculation and Rationalization of PKa Values. *J. Chem. Theory Comput.* 7 (7), 2284–2295.

(45) Olsson, M. H. M., Søndergaard, C. R., Rostkowski, M., and Jensen, J. H. (2011) PROPKA3: Consistent Treatment of Internal and Surface Residues in Empirical PKa Predictions. *J. Chem. Theory Comput.* 7 (2), 525–537.

(46) Lindorff-Larsen, K., Piana, S., Palmo, K., Maragakis, P., Klepeis, J. L., Dror, R. O., and Shaw, D. E. (2010) Improved Side-Chain Torsion Potentials for the Amber Ff99SB Protein Force Field. *Proteins: Struct., Funct., Genet.* 78 (8), 1950–1958.

(47) Best, R. B., and Hummer, G. (2009) Optimized Molecular Dynamics Force Fields Applied to the Helix–Coil Transition of Polypeptides. *J. Phys. Chem. B* 113 (26), 9004–9015.

(48) Wang, J., Wang, W., Kollman, P. A., and Case, D. A. (2006) Automatic Atom Type and Bond Type Perception in Molecular Mechanical Calculations. *J. Mol. Graphics Modell.* 25 (2), 247–260.

(49) Sousa da Silva, A. W., and Vranken, W. F. (2012) ACPYPE - AnteChamber PYthon Parser Interface. *BMC Res. Notes* 5 (1), 367.

(50) Jorgensen, W. L., Chandrasekhar, J., Madura, J. D., Impey, R. W., and Klein, M. L. (1983) Comparison of Simple Potential Functions for Simulating Liquid Water. *J. Chem. Phys.* 79 (2), 926–935.

(51) Bussi, G., Donadio, D., and Parrinello, M. (2007) Canonical Sampling through Velocity Rescaling. *J. Chem. Phys.* 126 (1), 014101.

(52) Berendsen, H. J. C., Postma, J. P. M., van Gunsteren, W. F., DiNola, A., and Haak, J. R. (1984) Molecular Dynamics with Coupling to an External Bath. *J. Chem. Phys.* 81 (8), 3684–3690.

(53) Parrinello, M., and Rahman, A. (1981) Polymorphic Transitions in Single Crystals: A New Molecular Dynamics Method. *J. Appl. Phys.* 52 (12), 7182–7190.

(54) Hess, B., Bekker, H., Berendsen, H. J. C., and Fraaije, J. G. E. M. (1997) LINCS: A Linear Constraint Solver for Molecular Simulations. *J. Comput. Chem.* 18 (12), 1463–1472.

(55) Humphrey, W., Dalke, A., and Schulten, K. (1996) VMD: Visual Molecular Dynamics. *J. Mol. Graphics* 14 (1), 33–38.

(56) Coffey, L. L., and Vignuzzi, M. (2011) Host Alternation of Chikungunya Virus Increases Fitness While Restricting Population Diversity and Adaptability to Novel Selective Pressures. *J. Virol.* 85 (2), 1025–1035.

(57) Pascual, M. J. M. J., Merwaiss, F., Leal, E., Quintana, M. E. M. E., Capozzo, A. V. A. V., Cavasotto, C. N. C. N., Bollini, M., and Alvarez, D. E. (2018) Structure-Based Drug Design for Envelope Protein E2 Uncovers a New Class of Bovine Viral Diarrhea Inhibitors That Block Virus Entry. *Antiviral Res.* 149 (Supplement C), 179–190.